International Journal of Multiphase Flow 34 (2008) 938–949

Contents lists available at ScienceDirect

International Journal of Multiphase Flow

journal homepage: www.elsevier.com/locate/ijmulflow

Sound generation on bubble coalescence following detachment

Richard Manasseh [a,*], Guillaume Riboux [b], Frédéric Risso [b]

[a] Fluid Dynamics Group, CSIRO[1] Materials Science and Engineering, P.O. Box 56, Highett, VIC 3190, Melbourne, Australia
[b] Institut de Mécanique des Fluides de Toulouse, UMR 5502 CNRS-INP-UPS, Allée Camille Soula, Toulouse 31400, France

ARTICLE INFO

Article history:
Received 11 February 2007
Received in revised form 27 March 2008
Available online 4 April 2008

Keywords:
Bubble
Acoustic
Sound emission
Coalescence

ABSTRACT

A system in which bubbles coalesced on formation was used to probe one mechanism by which bubbles create sound. The aim was to determine in which situations sound is produced and to predict its amplitude. A set of carefully co-ordinated high-speed video and acoustic timeseries showed that needle-formed bubbles generated loud bubble-acoustic emissions at the instant of coalescence of secondary bubbles with the primary bubble. As the air flow rate increased, the size and number of secondary bubbles increased, and the sound amplitude also increased. On coalescence, the sound pressure always rose initially. A dimensionless scaling found that the sound amplitude emitted scaled with the volume of the secondary bubble. This scaling was shown to be consistent with the sound-emission mechanism being the equalization of pressures in the coalescing bubbles. The trend in amplitude with bubble production rate was well predicted by the scaling.

1. Introduction

Gas bubbles can emit sound because the compressibility of the trapped gas and the mass of the surrounding liquid give rise to a natural oscillator. The compressible behaviour of bubbles has been studied for nearly a century (Rayleigh, 1917) and the natural frequency emitted by bubbles oscillating with small amplitude has been theoretically predicted and experimentally confirmed (Minnaert, 1933; Strasberg, 1953; Longuet-Higgins et al., 1991; Manasseh et al., 2004); it is usually called the Minnaert frequency. There are many contexts, such as sonoluminescence, in which a bubble is driven artificially to large amplitude by a known oscillating pressure or impulse, forcing nonlinear behaviour. However, there seems to be no universal explanation of the fluid-dynamical mechanism by which small-amplitude bubble sound emissions are naturally initiated. Thus, although there have been many studies that will be summarised below, there is still no accepted prediction of the sound amplitude naturally emitted by bubbles. Passive emission of small-amplitude sound by bubbles is common in many practical industrial flows (Hsi et al., 1985; Boyd and Varley, 2001; Manasseh et al., 2001) or environmental flows (Melville et al., 1988; Ding and Farmer, 1994; Manasseh et al., 2006). The emitted spectra depend on both the frequency and amplitude of the sources, and there is a need to invert the spectra to recover bubble-size distributions. There are many issues in interpreting the signals from such sources (e.g. Loewen and Melville, 1991a; Boyd and Varley, 2001; Manasseh et al., 2001), including the acoustic interactions between bubbles causing shifts in the resonant frequencies (Manasseh et al., 2004), that have led to increasingly complex signal-processing approaches (Al-Masry et al., 2005; Manasseh et al., 2006). Amongst the issues is the difficulty in relating the amplitude of the signal to its fluid-dynamical causes.

Longuet-Higgins (1990) proposed three general mechanisms by which the energy giving an initial acoustic perturbation could be imparted to the bubble: (i) a difference in instantaneous Laplace pressure at the instant the bubble is pinched off; (ii) the radial inrush of liquid as the pinch-off occurs; and (iii) an excitation of the volumetric or 'breathing' mode of the bubble by nonlinear interactions of shape modes (Longuet-Higgins, 1989a,b). It is likely that some of these mechanisms might work in some situations, but not in others (Leighton, 1994).

There are two broad classes of phenomena by which bubbles passively emitting sound are formed. The first class is when bubbles are pinched off from an underwater orifice connected to a large, parent body of gas. The formation process can be highly repeatable, particularly for moderate bubble-formation rates (Clift et al., 1978; Manasseh et al., 2001). Such bubbles can be formed very slowly (e.g. Longuet-Higgins et al., 1991), so that pressures inside the forming bubble and the parent body of gas are virtually identical, making mechanism (i) improbable. Yet they can make loud noises upon detachment. There have been a number of suggestions that the excitation mechanism for orifice-formed bubbles is a variant of (ii): it has been observed (Leighton, 1994) that a high-speed liquid jet penetrates the bubble on the breaking of the neck that joins it to its parent body of gas, and may be responsible

* Corresponding author. Tel.: +61 3 9252 6340; fax: +61 3 9252 6586.
E-mail addresses: Richard.Manasseh@csiro.au (R. Manasseh), riboux@imft.fr (G. Riboux), Frederic.Risso@imft.fr (F. Risso).
[1] CSIRO: Commonwealth Scientific and Industrial Research Organisation.

0301-9322/$ - see front matter
doi:10.1016/j.ijmultiphaseflow.2008.03.005

for compressing the trapped gas (Manasseh et al., 1998). Recent progress has been made in predicting the sound-emission mechanism in bubble pinch-off (Deane and Czerski, in press).

Longuet-Higgins et al. (1991) proposed that orifice-formed bubbles could make sound by mechanism (iii). At detachment, the distortion away from a bubble's equilibrium spherical shape is severe, and could be decomposed into a large number of shape eigenmodes, some of which would match the criteria for nonlinear interaction (Longuet-Higgins, 1989b). A precise resonance condition is required. Only a fraction of the total potential energy due to the surface distortion would be projected onto the modes capable of nonlinearly driving the volumetric mode. Furthermore, these theories do not readily yield quantitative predictions of sound amplitude for comparison with experiments. Numerical simulations of compressible multiphase flows, while advancing in quality (e.g. Oğuz and Prosperetti, 1993; Hu and Khoo, 2004; Bui and Manasseh, 2006) and offering many insights (Prosperetti and Oğuz, 1993) remain as ambivalent as laboratory experiments on the actual excitation mechanism.

The second class of bubble-formation phenomena is when bubbles are created by the entrapment of air from a free surface, which might occur in contexts such as raindrop impact (e.g. Pumphrey and Elmore, 1990; Pumphrey and Crum, 1990), a plunging jet (e.g. Hahn et al., 2003; Chanson and Manasseh, 2003) or wave-breaking (e.g. Melville et al., 1988; Loewen and Melville, 1991a,b; Ding and Farmer, 1994; Manasseh et al., 2006). At the instant the surface closes, pinching off the bubble, there must be a sudden transition from a cavity at atmospheric pressure to a closed bubble in which the pressure exceeds atmospheric by the Laplace pressure due to surface tension, plus the hydrostatic pressure that must now be supported. Thus, in this second class of phenomena, mechanism (i) is a possible explanation as well as (ii) and (iii).

Pumphrey and Elmore (1990) created bubbles from drop impacts in the laboratory, estimated the bubble size photographically and measured the amplitude of sound emitted. They calculated the Laplace pressure in the newly-formed bubble (and also the hydrostatic pressure, which was small in comparison). Because the newly-formed bubble in their experiment was just below a surface, it was necessary to consider the acoustic field as dipolar. Comparisons with experiment were disappointing, with the predicted dipole strength at best 25% of the experimental values. Theory predicted a dipole strength increasing linearly with bubble resonant frequency. An increase was observed experimentally, though it was not linear. In contrast to pinch-off experiments, drop-impact studies are complex, and statistical confidence harder to obtain, because there is considerable variation from drop to drop owing to the natural variation in impact conditions.

The present paper reports experiments in which bubbles emit sound on coalescence. These bubbles are formed by the first class of phenomena, pinch-off from an orifice. Orifice-formed bubbles have been noted before to emit loud sounds on coalescence (Leighton et al., 1991), which can dominate the sound spectrum provided the system is not highly turbulent (Chen et al., 2003). Depending on the air flow rate through the orifice, zero, one, or several coalescences might occur between a newly-formed bubble and the previously-formed bubble immediately above it. All mechanisms (i), (ii) and (iii) are conceivable in this case. The present experiments are easier to control and hence more repeatable than the complex drop-impact phenomena that have been the subject of extensive investigation before. Careful co-ordination of acoustic and high-speed video data logging enabled a direct comparison of the interfacial kinematics with the acoustic pressure trace. Thus, it may be that experiments on this system could lead to a better elucidation of the excitation mechanism.

2. Experimental system

2.1. Equipment

The general layout of the experiment is shown in Fig. 1. The test section is a glass tank 1000 mm high with a square cross-section of 150 mm. The tank is filled with filtered tap water at a temperature between 16 and 17 °C. Air bubbles of 1.6 mm diameter are injected at 85 mm from the bottom of the tank by a needle with an internal diameter of 0.1 mm and a length L_c = 100 mm. The needle was fitted directly into the tank bottom plate. The rate of bubble production is controlled by adjusting the pressure in the tank to which the needle is connected.

A high-speed digital video camera (Photron Ultima APX) is used to film the bubble detachment from the tip of the needle at a frame rate of 20,000 Hz and with an exposure time of 1/87,600 s. The filmed region, 1.113 mm high and 2.226 mm width, is described by 128 × 256 pixels. Images of the bubbles were processed to extract their equivalent-spherical radius and location as a function of time (details on the procedure are available in Ellingsen and Risso (2001)).

A Brüel & Kjaer type 8103 hydrophone was used to transduce the acoustic signal. In the relevant 1–10 kHz band, this hydrophone type has an essentially spherical directivity field, ensuring sounds from any direction are equally transduced. The hydrophone response is flat up to 15 kHz (Brüel and Kjaer, 2007), enabling a linear conversion from transduced voltage to pressure based on the hydrophone's individual calibration. To correctly translate voltage to pressure it must be noted that the Brüel & Kjaer 8103 inverts the polarity of the pressure signal.[2] The location of the hydrophone relative to the needle was measured with an accuracy of ±0.1 mm by taking images in two orthogonal directions. Distances were calculated from the true acoustic centre of the 9.5 mm diameter hydrophone. In the present experiments the distance from the acoustic centre to the bubble centre was 19.1 ± 0.1 mm. The hydrophone's presence caused no disturbance to the bubble formation and rise dynamics.

The hydrophone signal was pre-amplified by Brüel & Kjaer type 2635 charge amplifier set to the individual calibration of the hydrophone. The signal was then fed through a purpose-built high-pass 5-pole Bessel filter with a 500 Hz cut-off and an amplitude gain of 10. The high-pass filtering eliminated any low-frequency pressure fluctuations due to bubble motion while preserving completely the bubble-acoustic signals which were all above 3 kHz. The filtered signal was digitized by a National Instruments Data Acquisition Card type 6024E using high-speed data logging software built on the National Instruments LabView platform. Considering the typical level of background noise, the random error in transduction of the acoustic pressure was less than 10%. This could be improved if necessary with low-pass filtering, but for the comparisons of the present paper this accuracy was sufficient.

The gate signal from the camera was logged on one channel of the datalogging card and the high-pass filtered acoustic signal was logged on a second channel. A nominal logging rate of 120 kHz was used for both channels. However, since a precise comparison of the video and acoustic signals was required, it was noted that no card will in fact digitize data at exactly the requested rate but at a marginally different rate dependent on the card's internal arithmetic; in the present experiments this marginal difference is sufficient to cause a noticeable misalignment of acoustic and video records for the lowest bubble production rates. The actual logging rate was extracted from low-level rou-

[2] M. Ruzicka and R. Buganic 2004, pers. comm.

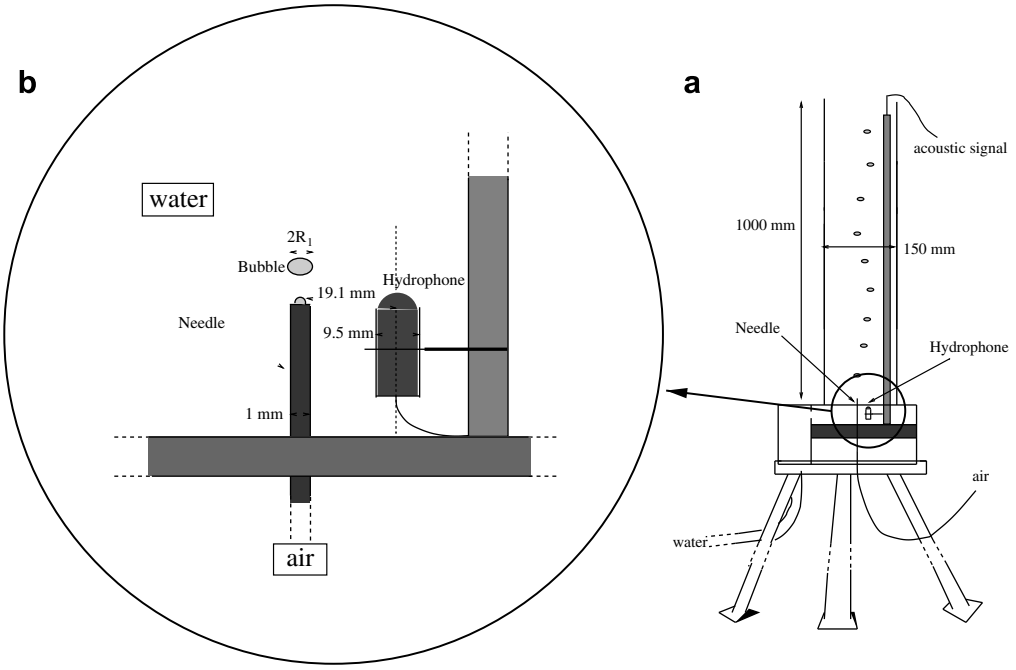

Fig. 1. Schematic of the experimental set-up. (a) Tank and air supply. (b) Bubble formation and hydrophone.

tines and was found to be 119,760.48 Hz; its use ensured a comprehensively precise comparison of acoustic and video records.

2.2. Sound field in the tank

Reflections of sound must occur from the walls of the tank and would return to the bubble from the nearest walls in only 50 μs. Reflections could influence not only the signal, but be coupled with the bubble dynamics, effectively creating an entirely different oscillatory system to that which would be found if the walls were infinitely far away (Leighton et al., 1998, 2002; Farmer et al., 2005). As the tank in which bubbles are formed is made smaller, an effect on the acoustic signal can be noted (Nikolovska, 2005), although this problem is most marked with tanks of circular rather than square cross-section.

Tests were done in a tank with much larger horizontal dimensions, as detailed in Table 1. The bubble-forming nozzle and hydrophone were fixed to the same support which was simply moved as a fixed item into the larger tank. The bubble production rate was adjusted to be the same in both the larger test tank and the actual experimental tank, about 4 Hz (a condition at which coalescence and loud bubble-acoustic emissions occur repeatably, as detailed in Section 3.1). There was no significant difference to the pulse on the oscilloscope (a typical example, to be discussed later, is Fig. 9a) and points on the pulse waveform were measured to illustrate this (Table 1).

It should be noted that a bubble chain itself will cause an anisotropy in the sound field. This is due to the acoustic coupling of the bubbles, a phenomenon which has been well studied (e.g. Zabolotskaya, 1984; Tolstoy, 1986; Prosperetti, 1988; Doinikov and Zavtrak, 1995; Feuillade, 2001; Hsiao et al., 2001; Ida, 2002). In the present experiment the bubbles in the chain are the same size and so resonate at the same frequency as the newly-formed and just-coalesced bubble, allowing sound to be efficiently re-transmitted along the chain. However, this effect is manifested over several multiples of the spacing between bubbles (Manasseh et al., 2004; Doinikov et al., 2005; Nikolovska et al., 2007) and the hydrophone in the present experiments was less than one spacing away.

To check the sound field in the tank, a hydrophone was first traversed in both horizontal and vertical directions away from the bubble-formation point. The bubbling rate f_b was 14 Hz. Locating the 9.5 mm diameter hydrophone closer to the bubble than about 15–20 mm ran the risk of distorting the fluid flow associated with the bubble production. Fig. 2 shows the distribution of sound amplitude with distance. The sound field in the horizontal direction (along which the hydrophone was located for the experiments that are the subject of this paper) can be fitted by a function of the form $r^{-1.09}$ with a correlation co-efficient R^2 of 0.99. As noted, the vertical profile should not be expected to decay as $1/r$, and the data can be fitted by a function of the form $r^{-0.82}$ with $R^2 = 0.99$. The difference in the far-field exponents of the horizontal and vertical is consistent with data and theory already published on this topic (Manasseh et al., 2004; Doinikov et al., 2005; Nikolovska et al., 2007).

In summary, in the experiments that are the subject of this paper, the simplest approximation to the sound field consistent with the data is a monopole i.e., the pressure amplitude falling as r^{-1}

Table 1
Comparison of the acoustic pulse produced from the 0.1 mm internal diameter needle in different tanks, bubble production at 4 Hz (for an example, see Fig. 9a)

Tank	Length (mm)	Span (mm)	Depth (ms)	T1 (ms)	T5 (ms)	T8 (ms)	V1 (mV)	V8 (mV)
Actual experimental	150	150	1000	0.23	1.16	1.85	70	16
Large horizontal	370	650	410	0.24	1.19	1.80	68	14

T1: time interval between the first and second peaks; T5: time between the first and fifth peaks; T8: time between the first and eighth peaks; V1: amplitude of first peak; V8: amplitude of eighth peak.

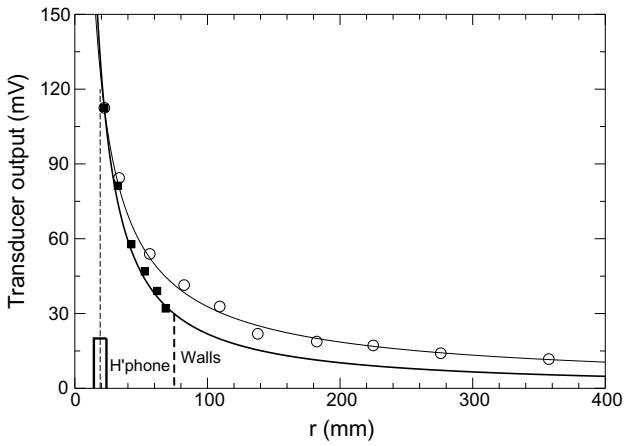

Fig. 2. Sound amplitude as a function of horizontal distance (rectangular symbols) and vertical distance (circles) from the bubble centre. Amplitude is raw voltage output from the charge amplifier without filtering. Curves are fits to the data with exponents $r^{-1.09}$ for horizontal data and $r^{-0.82}$ for vertical data. Vertical dashed lines show hydrophone location for the experiments reported in this paper, and the location of the side wall. Block on horizontal axis indicates width of hydrophone.

with distance. Caution must be exercised in making a comparison of the data with any theory that assumes walls are infinitely far away.

3. Experimental results

3.1. Inception of sound emission on coalescence

At very low bubble production rates, less than 3.5 s^{-1}, a series of single bubbles is formed: high-speed imaging confirms there is no coalescence. A very faint signal is detectable on amplification of the hydrophone signal, barely above the background noise, corresponding to the pinch-off of each bubble. It is interesting to note that these bubbles are approximately 1.6 mm in diameter. The bubbles of Manasseh et al. (2001), which made noises audible by the unaided ear on pinch-off, ranged from about 4 to 8 mm in diameter and hence were one to two orders of magnitude larger in volume. Once the air flow rate is increased such that the bubbling rate f_b is above 3.6 ± 0.1 s^{-1}, occasional loud clicks are audible and corresponding sharp spikes appear on an oscilloscope trace. These spikes have an order of magnitude greater amplitude than the sound created on pinch-off. The frequency was 4.15 ± 0.5 kHz which is the Minnaert frequency for a bubble of 1.6 mm diameter. Above an air flow rate of 3.8 ± 0.1 s^{-1}, loud clicks are produced regularly and the spikes are spaced regularly at the bubble production rate. The 3.8 ± 0.1 s^{-1} threshold for this phenomenon was repeatable in separate experiments performed over several different days.

The acoustic record over a time window of 300 ms is shown in Fig. 3. The pressure recorded at the hydrophone location is sufficient for the simple comparisons of the present paper. However, theoretical calculations are generally based on the pressure at the bubble surface. Hence, to aid comparisons with future theoretical work, in the present paper all measured pressures have been translated to the pressure at the bubble surface. Based on the measured $1/r$ dependence in the horizontal (Section 2.2), a simple scaling factor d/R_1 is used for the translation, where d is the distance from the bubble centre calculated from the video image to the hydrophone acoustic centre; for the present experiments $d/R_1 = 23.26$. Bubbles are formed from the needle at 3.8 s^{-1}; about 260 ms apart. There is a series of sound pulses, with an order of magnitude amplitude difference from the background. Each pulse is audible as a single 'tap' or 'knock' like an individual musical note

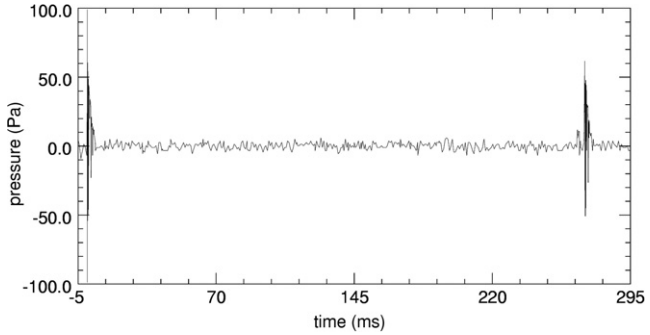

Fig. 3. Timeseries of acoustic pressure at bubble surface over a time of 300 ms. Bubble production rate 3.82 ± 0.03 s^{-1}. Series triggered on a pulse at time $t = 0$. Data logged at 120 kHz.

being struck, and thus is like any individual bubble-acoustic pulse reported in the literature (e.g. Minnaert, 1933; Strasberg, 1956; Leighton and Walton, 1987; Manasseh et al., 2001). In reality, close observation of the high-speed video (Fig. 4) shows that a smaller secondary bubble forms immediately after the primary has detached, and soon thereafter coalesces with it. The secondary bubble is much smaller, being at this air flow a sixth the diameter of the primary. It coalesces with the primary before it has detached itself, thus temporarily re-attaching the primary to the air supply. About 0.1 ms later, it detaches itself and is absorbed into the primary. The size of the bubbles are quite repeatable.

The circumstances leading to in-line pairing and subsequent coalescence of orifice-formed bubbles have been studied before (Nevers and Wu, 1971; Bhaga and Weber, 1980; Stewart, 1995; Manasseh, 1996); although most detailed studies are for the pairing and coalescence of equal-sized bubbles. While this phenomenon of coalescence at the orifice is certainly well known to occur, acoustic studies do not seem to have been made.

Thus, each of the "3.8 bubbles per second" is really a primary that has coalesced with a secondary immediately following, so that over a long time scale they appear to be one bubble. Each formation-and-coalescence event is heard as a single sound pulse. Over the 300 ms timescale, the second formation-and-coalescence event appears as a second pulse about 260 ms later. Most significantly, the sound created on coalescence has an order of magnitude greater amplitude than the sound created on pinch-off.

A digital oscilloscope (Tektronics TDS210) enabled a measurement of the rate of production of primary bubbles, by measuring the interval between pulses. Typically, this could be done with an accuracy of ±0.1 s^{-1} or less; however, as noted below, for the highest bubble production rates the bubble formation became less regular, giving a bubble production rate estimation accuracy of ±0.5 s^{-1}. In the calculations of Section 4 the primary bubble will be denoted with the subscript '1' and the secondary with the subscript '2', so that, for example, the equivalent-spherical radii of the primary and secondary bubbles will be denoted as R_1 and R_2 respectively.

3.2. Behaviour as air flow rate is increased

As the air flow rate is increased, further coalescences occur with each primary bubble, with the number of coalescences increasing with air flow rate and each coalescence regime being quite repeatable. Like the binary in-line coalescences noted above, multiple coalescences at a needle tip have been observed before with photographic techniques (e.g. Leighton et al., 1991; Yoshida et al., 1998). The production of the primary bubble and all following bubbles that coalesce with it are still clearly separated in time from the production of the next primary bubble. Thus the 'bubbling rate' f_b quoted throughout the present paper is the rate of production of

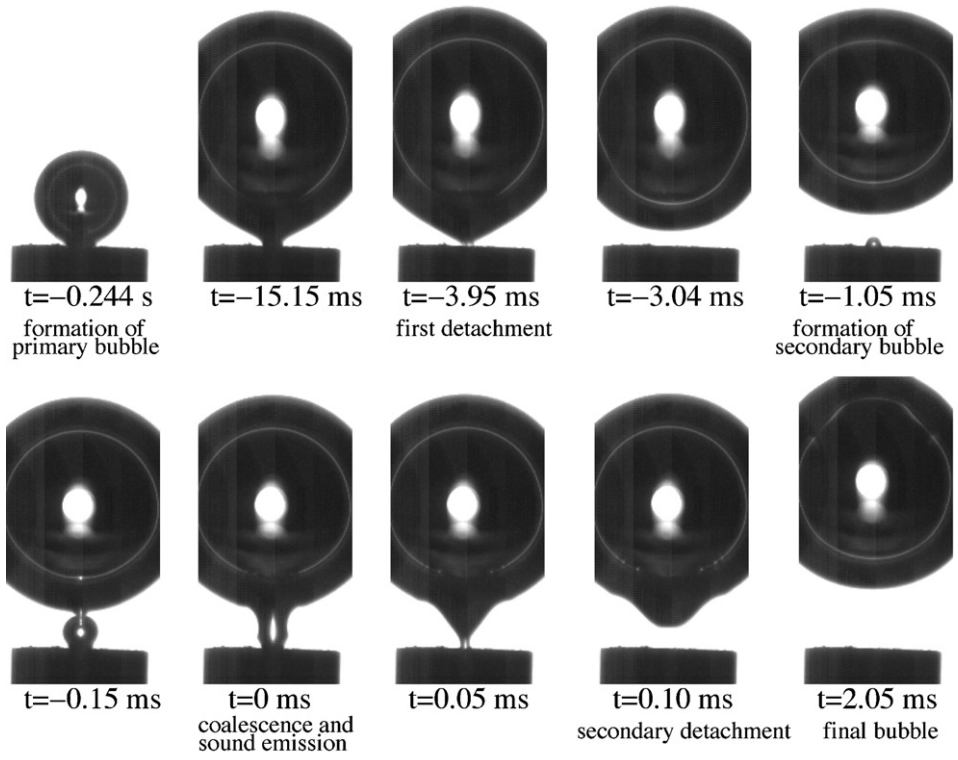

Fig. 4. Bubble-formation sequence. Bubble production rate 3.82 ± 0.03 s^{-1}, bubble diameter 1.6 mm.

primary bubbles. For the present experiment, the number of coalescences as a function of the bubbling rate f_b is shown in Fig. 5. As air flow rate is incremented, a new regime appears in which a new secondary bubble just 'kisses' the primary, i.e. it appears to be separated from it by a thin film, but does not coalesce and thereafter separates; on a further slight increment in air flow rate it will coalesce.

At a bubbling rate of 25 ± 0.5 s^{-1}, up to nine coalescences were observed in the high-speed video data; in this case each of the "25 bubbles per second" is really a bubble formed from the merging of 10 bubbles. Above 25 ± 0.5 s^{-1} bubble production becomes chaotic.

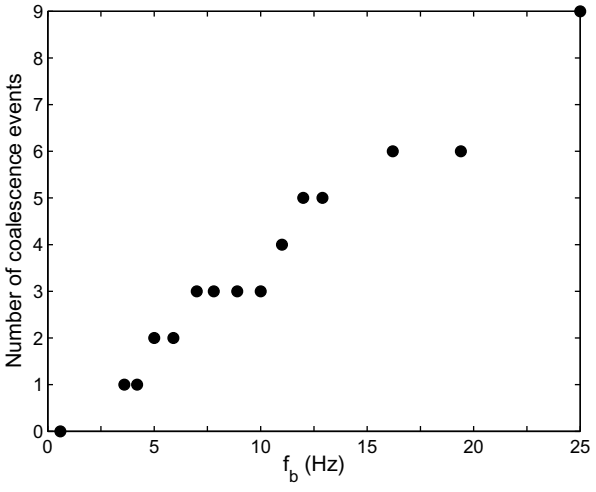

Fig. 5. Number of coalescences of smaller following bubbles with the primary bubble, as a function of the rate of production of primary bubbles (the 'bubbling rate'), f_b.

Co-ordinated acoustic and video data were taken at 14 bubble production rates, from 3.8 to 25 s^{-1}. The timeseries of acoustic pulses for a few of these cases are shown in Figs. 6 and 7. Sound amplitude increases with air flow rate, a phenomenon that forms the basis of the present study and will be discussed in detail in Section 4.

3.3. Detailed comparison of high-speed video and acoustic data

Acoustic timeseries and photo-montages of the high-speed video frames were generated over the same time window so that acoustic and visual events could be clearly correlated. A variety of time window lengths were used. The photo-montages were created as follows. The original size of the frames, which can be seen in Fig. 4, was 128 pixels wide by 256 pixels high. Given the desired time window and the number of frames available within that time, the width was calculated of a vertical 'strip' of the centre of each frame. For example, if a time window required 100 frames to fit into a montaged image 400 pixels wide, a vertical strip with the central 4 pixels of each 128 pixel image was cut out and inserted into the montaged image at its corresponding time. Since most of the interesting variations occur on the centreline of the bubble image, this technique preserved much of the relevant information content of the high-speed video. In the extreme, a montage of strips each only 1 pixel wide would be a 'time–space diagram' (e.g. Goharzadeh and Mutabazi, 2001) showing the rate at which events move along the centreline.

The time $t = 0$ has been set at the centre time of the frame where coalescence of the primary and first secondary bubble occurs. Progressively higher time-resolution plots of the same data, shown in Figs. 8–10, will now be described.

In Fig. 8, the time window has in expanded detail the 10 ms around the first coalescence event. Using this window, the montaged video frames are reduced to only a few pixels' width, giving

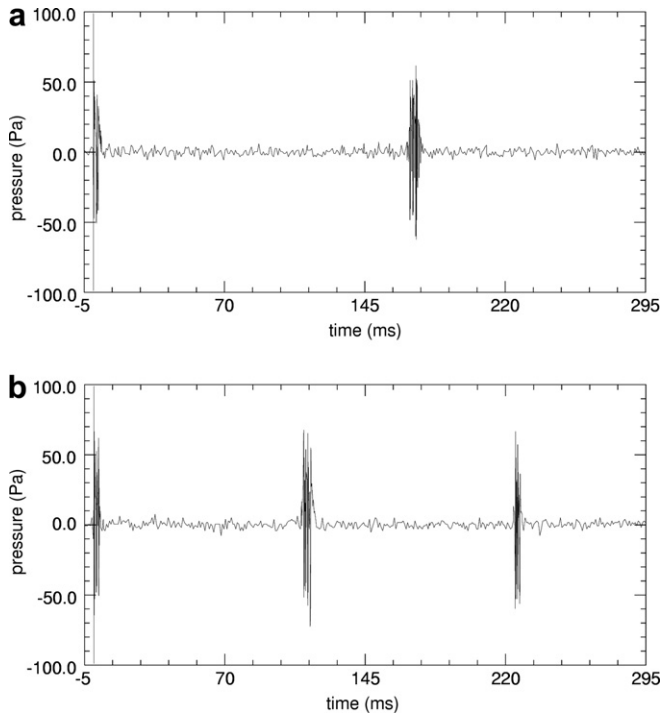

Fig. 6. Timeseries of acoustic pressure at bubble surface over a time of 300 ms. Bubble production rates (a) $5.92 \pm 0.05\ s^{-1}$; (b) $8.9 \pm 0.1\ s^{-1}$. Series triggered on a pulse at time $t = 0$. Data logged at 120 kHz.

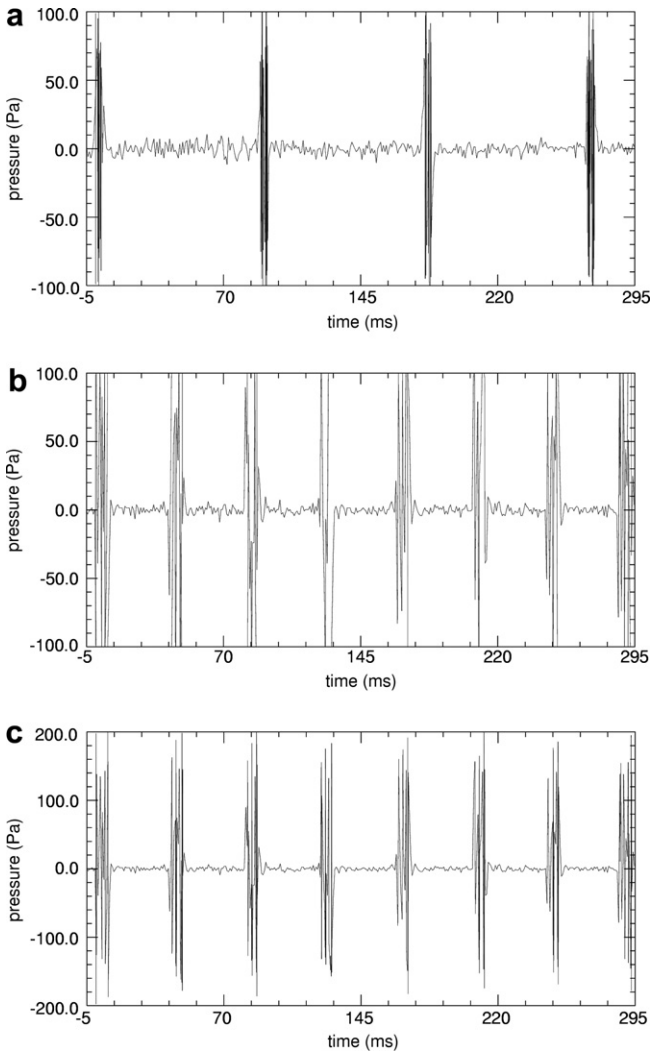

Fig. 7. Timeseries of acoustic pressure at bubble surface over a time of 300 ms. Bubble production rates (a) $11.1 \pm 0.1\ s^{-1}$; (b) $25.0 \pm 0.5\ s^{-1}$; (c) as (b), with expanded pressure scale. Series triggered on a pulse at time $t = 0$. Data logged at 120 kHz.

an approximate 'time–space diagram'. In the time–space diagram for the $3.8\ s^{-1}$ bubbling rate (upper panel of Fig. 8a), the detachment of the primary bubble at approximately −4.0 ms can be seen as the appearance of the white gap between the bottom of the primary bubble and the needle tip; some corresponding low-amplitude sound emission occurs, which as already noted is only slightly higher than the background noise. The bottom of the primary bubble appears to rise approximately linearly over the next few milliseconds. The low-amplitude detachment-noise falls off. The growth of the secondary bubble can be seen from approximately −1.0 ms up to its coalescence at 0.0 ms and co-incident sound emission, which as already noted is much larger (by roughly a factor of 8) than the detachment sound.

A further secondary bubble starts to grow at about 2.5 ms. Similar behaviour can be seen for the higher bubbling rates. In Fig. 8b there is a second coalescence event and a second sound pulse, but the third secondary bubble just 'kisses' so there is no sound emission. In Fig. 8c there are clearly three coalescences and three sound pulses; the fourth secondary 'kisses'.

In Fig. 9, the time window has in expanded detail the 4 ms around the first coalescence event. In the montaged video frames in Fig. 9a, the rate of growth of the secondary bubble appears to approximately follow a $t^{1/n}$ function; a constant air flow rate from the needle would correspond to a $t^{1/3}$ function. The acoustic timeseries show the sound pulse commencing at the time of coalescence. The maximum and minimum peaks on these timeseries were used to calculate the amplitude of the acoustic pressure, P_{ac} according to $P_{ac} = \frac{1}{2}(P_{max} - P_{min})$. The sound pressure always rises at the start of the pulse.

In Fig. 9b–d, the further coalescences at higher bubbling rates can be seen in more detail than in Fig. 8b–d. It is clear that there is an abrupt change in the acoustic signal initiated at each coalescence event. In all cases the sound amplitude on coalescence is much larger than the sound created on detachment.

Finally, in Fig. 10, the time window has in expanded detail the 1 ms bracketing the first coalescence event. Again, the clearest situation is the lowest bubble production rate shown in Fig. 9a. It is now quite clear that the sound pulse is initiated at the very instant of coalescence. It can be noted that prior to sound production, the primary bubble begins to develop a small, downward-pointing 'nose' in response to the approach of the secondary bubble. (We know of no purely hydrodynamical mechanism that can explain this 'nose', which might be related to the presence of surfactants or electric effects. For example, as the bubbles approach, increased flow in the narrowing liquid bridge between them may create gradients in surface tension by advection of surface contaminants.) It is clear that sound pressure rises during the coalescence event.

3.4. Summary of observations

Some sound is produced on the detachment of the primary bubble from its parent body of gas in the needle. However, the production of high-amplitude sound, and hence the majority of the sound power measured, coincides as closely as we can measure with the instant of coalescence of secondary bubbles with the primary bubble. As the air flow rate increases, the size and number of secondary bubbles increases, and the sound

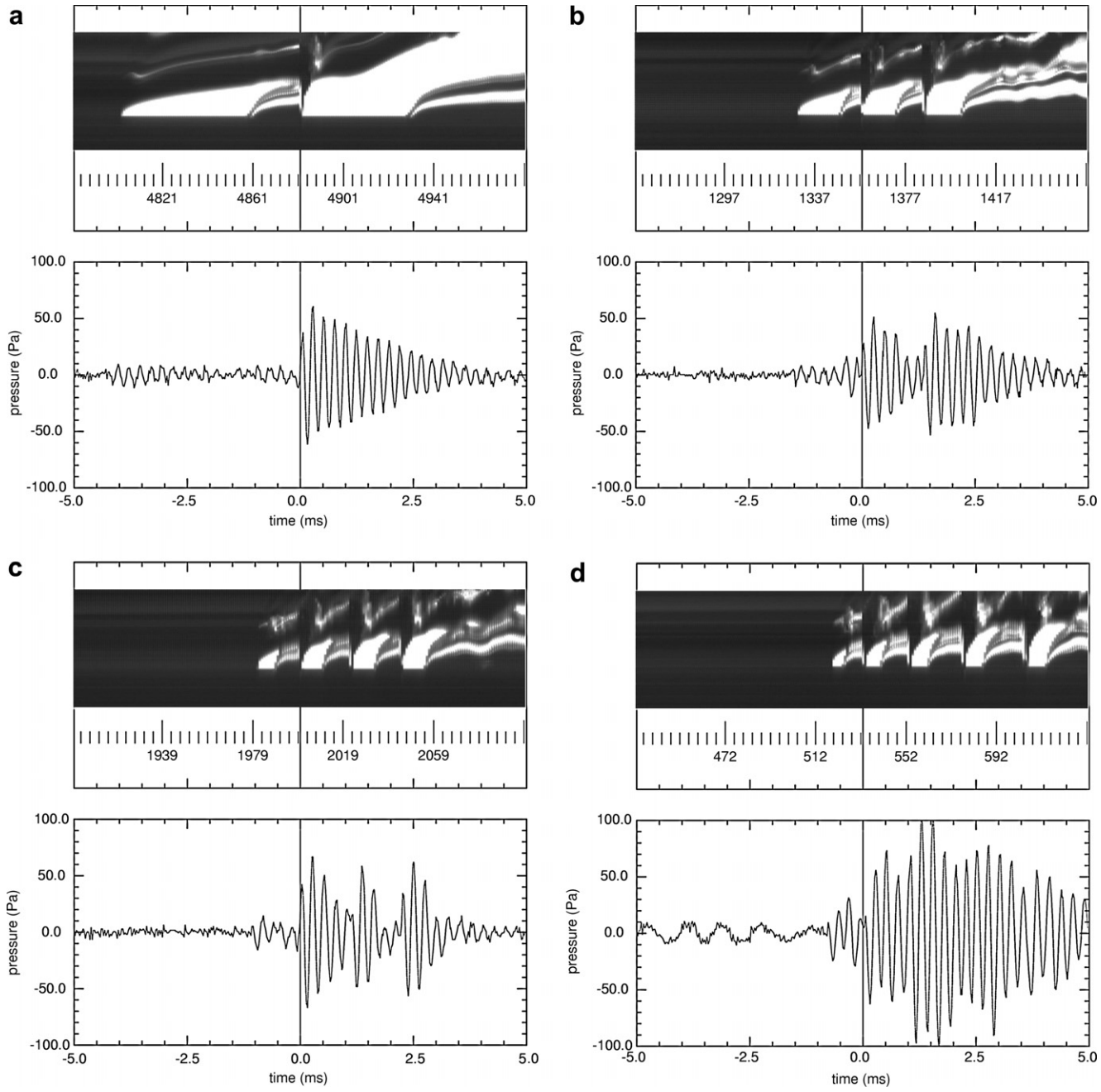

Fig. 8. Timeseries of video and acoustic data over a time of 10 ms. Bubble production rates f_b are (a) 3.8 s^{-1}; (b) 5.9 s^{-1}; (c) 8.9 s^{-1}; (d) 11.1 s^{-1}. Secondary scale in upper panels shows video frame numbers. Video data logged at 20 kHz; acoustic data at 120 kHz. As in previous figures acoustic pressure has been translated to bubble surface.

amplitude also increases. On coalescence, the sound pressure always rises initially.

Different time scales can be introduced based on the observations,

- time for equilibrating pressure in the large bubble, $t_c = 2R_{1/c} \approx 10^{-6}$ s (where c is the speed of sound);
- time for sound reflected from the wall to return to the bubble, $t_r \approx 10^{-4}$ s;
- period of bubble-acoustic oscillation, $t_a \approx 10^{-4}$ s;
- time required for the small bubble to disappear in the large one, $t_{cf} \approx 5 \times 10^{-4}$ s;
- duration of the acoustic emission, $t_e \approx 5 \times 10^{-3}$ s;
- time interval between two successive primary bubbles, $t_b = 1/f_b \approx 10^{-1}$ s.

The timescales relevant to the initiation of sound emission are of different orders of magnitude, namely $t_c \ll t_r \simeq t_a < t_{cf} \ll t_e \ll t_b$.

At the instant the film of water that initially separates the bubbles breaks, two volumes of gas at different pressures are suddenly put into contact. The two pressures equalize in a very short time ($t_c \approx 10^{-6}$ s) during which the bubble volume and shape are frozen. Then, the bubble volume starts oscillating and sound is emitted. A few oscillation periods ($t_a \approx 10^{-4}$ s) pass before the secondary bubble has time to disappear into the large primary bubble ($t_{cf} \approx 5 \times 10^{-4}$ s). Volume oscillations last quite a long time ($t_e \approx 5 \times 10^{-3}$ s,) after the shape of the resulting bubble has been stabilized. Depending on the gas flow rate, several other secondary bubbles may be formed and coalesce with the large bubble before acoustic emissions end. But in any case, the large bubble has time

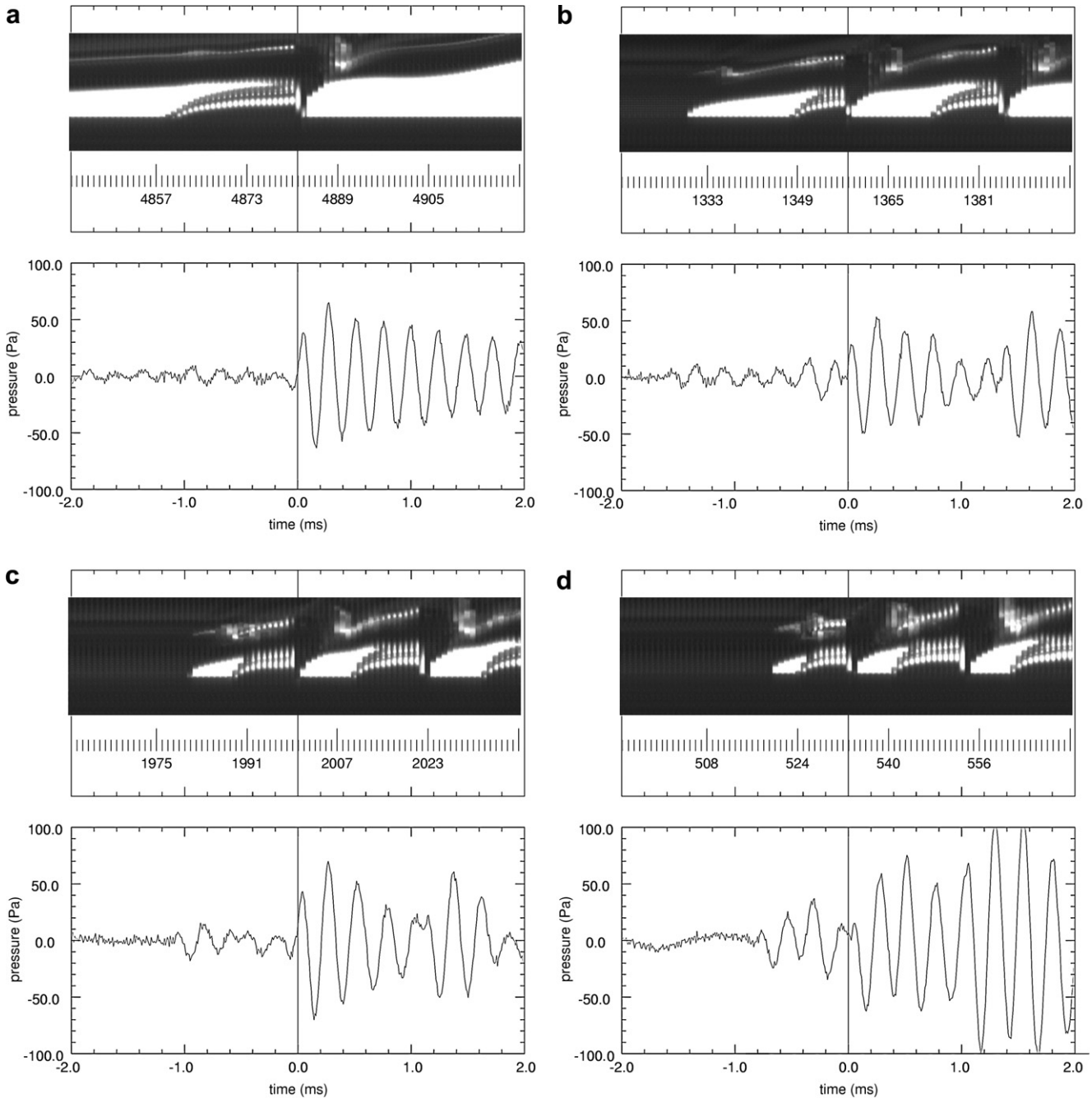

Fig. 9. Timeseries of video and acoustic data over a time of 4 ms. As for Fig. 8, bubble production rates f_b are (a) 3.8 s^{-1}; (b) 5.9 s^{-1}; (c) 8.9 s^{-1}; (d) 11.1 s^{-1}. Secondary scale in upper panels shows video frame numbers. Video data logged at 20 kHz; acoustic data at 120 kHz. As in previous figures acoustic pressure has been translated to bubble surface.

to travel far from the needle and sound has been damped before another primary large bubble is formed at $t_b \approx 10^{-1}$ s.

In the following section the amplitude of the sound produced on coalescence will be analysed to see if a version of the Laplace-pressure-equalization mechanism employed by Pumphrey and Elmore (1990) is consistent with the cause of the sound emission observed in the present experiments.

4. Scaling of the sound amplitude

Several physical parameters control the whole problem of detachment and sound emission. Amongst them are the air flow rate Q, the needle inner diameter d_c and its length L_c, the pressure P_t in the air tank to which the needle is connected, the surface tension σ, the liquid density ρ_l, the gas density ρ_g and the ambient pressure P_0.

The images yield the equivalent-spherical radii of the primary bubble R_1, the smaller secondary bubble at the time it attached to the first bubble, R_{21}, and the secondary bubble at the time it detached from the needle, R_{22}. These radii are calculated following the method of Ellingsen and Risso (2001).

The parameters Q, d_c, L_c and P_t will control the bubbling rate f_b, the various bubble sizes R_i, the number of coalescences, and so on. A range of empirical and theoretical studies is available on the topic of bubble formation (detailed in Clift et al., 1978) controlled

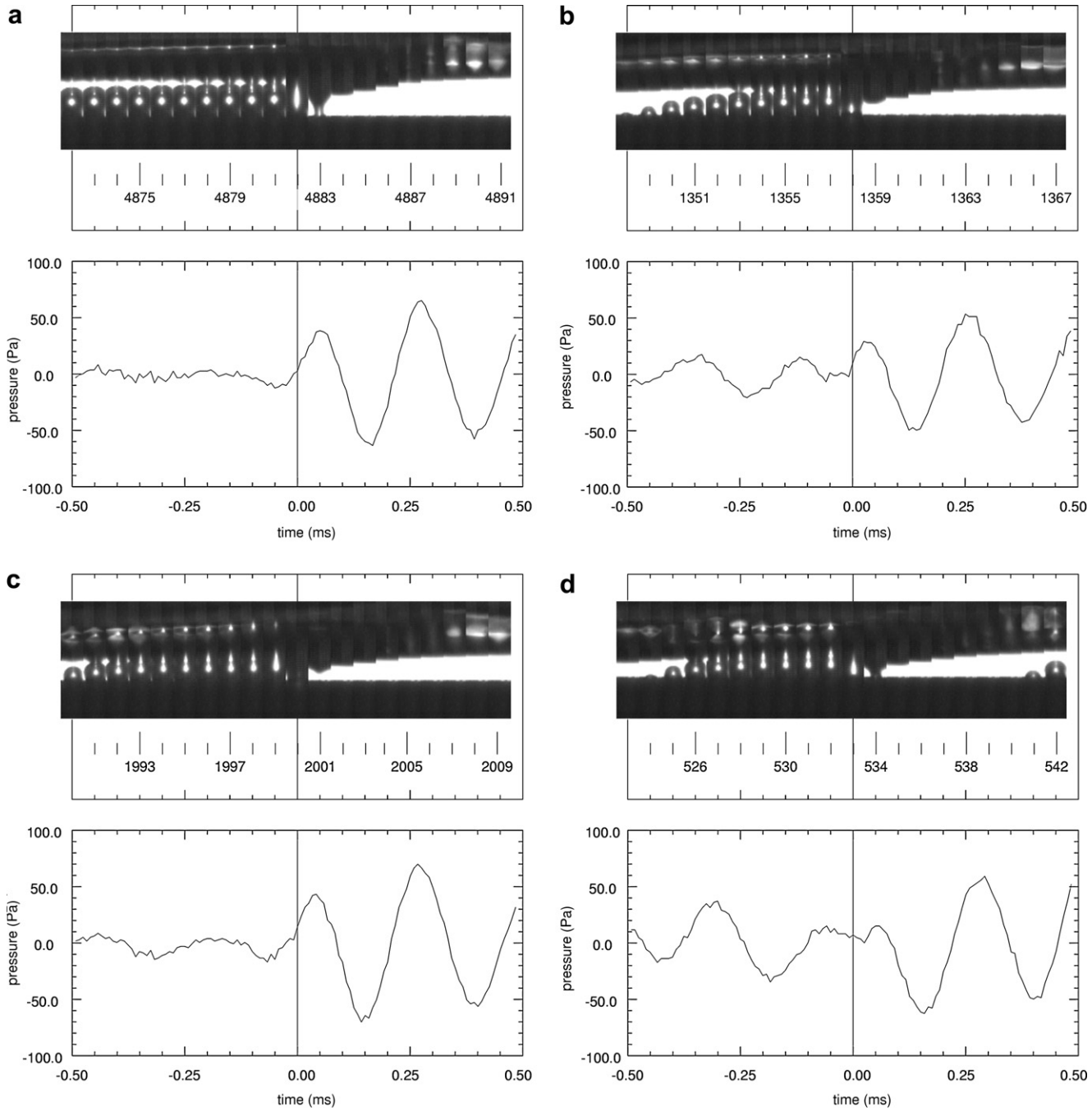

Fig. 10. Timeseries of video and acoustic data over a time of 1 ms. As for Fig. 8, bubble production rates f_b are (a) 3.8 s^{-1}; (b) 5.9 s^{-1}; (c) 8.9 s^{-1}; (d) 11.1 s^{-1}. Secondary scale in upper panels shows video frame numbers. Video data logged at 20 kHz; acoustic data at 120 kHz. As in previous figures acoustic pressure has been translated to bubble surface.

by these parameters, but it is the amplitude of sound emission that is of present interest.

Firstly, consider the experimental acoustic measurement which is shown in Fig. 11. The amplitude of sound emitted clearly trends upwards with f_b. In these experiments, the trend was not monotonic, first falling to a minimum at $f_b \simeq 5$ Hz, then rising to an intermediate peak at $f_b \simeq 10$ Hz, then falling again before continuing to rise.

The present experiments were in a regime where increases in air flow rate are manifested in increased bubble production rate without significant changes in primary bubble size (e.g. Clift et al., 1978). Increases in the radius of the primary bubble could not be measured within the accuracy of the video system. The secondary bubble has a volume that is never more than 1% of the primary bubble volume, so the primary bubble radius (and hence its acoustic frequency) is changed by a factor smaller than the cube root of 1% after coalescence. This is why, even after coalescence, the different secondary bubble sizes caused a negligible change in the primary bubble size.

Prior to making any assumptions, consider the simplest dimensionless parameter, R_2/R_1. Since R_2 is a rapidly-varying function of time, consider only two values, R_{2i}, where $i = 1, 2$ give the values of R_2 measured from video frames at coalescence and immediately after coalescence. Since the measurements are only made from the videos frames just at and just after coalescence, there is no meaning to R_{2i} later in the evolution of the coalesced bubble.

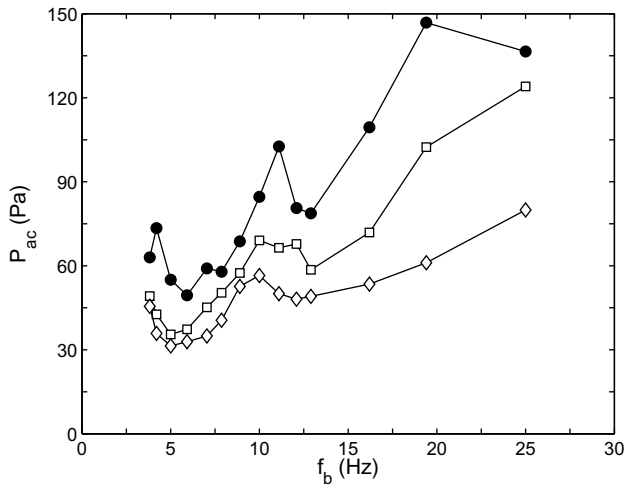

Fig. 11. Acoustic pressure P_{ac} at bubble surface and dimensionless variables vs. bubbling frequency: ●, P_{ac}; □, $C\alpha_V \equiv \alpha_{R2}^3 = (R_{22}/R_1)^3$; ◇, $C\alpha_{R1}^3 = (R_{21}/R_1)^3$. (The arbitrary constant $C = 10^4$ Pa is used to get dimensionless variables on the same scale as P_{ac}).

Calculations can be made using $\alpha_{Ri} \equiv R_{2i}/R_1$ and also the powers of α_{Ri}. Of course, α_{Ri}^2 is the surface area ratio of the small to the large bubble and α_{Ri}^3 is the volume ratio. Moreover, in these experiments the large bubble's radius R_1 is virtually constant, so any variation in these ratios is simply the variation in the small bubble's size.

The open symbols in Fig. 11 show the variation of the volume ratios. It is widely reported in the chemical engineering literature that as volume flow rate increases, the rate of production of primary and secondary bubbles, and their size, do not necessarily increase monotonically (Clift et al., 1978). It is clear that the volume ratio, particularly that of the final size of the small bubble α_{R2}^3, gives a very reasonable match to the experimental trend. Both the initial drop and the intermediate peak are reproduced at the correct f_b. (Defining the radius of the final coalesced bubble as R_3, the ratio R_{22}^3/R_3^3 could be plotted as an alternative, but that barely makes any difference since $R_1^3/R_3^3 \simeq 1$ as shown below; in fact only the last data point is shifted very slightly, by less than the size of the symbol.) From now on α_V will denote the ratio R_{22}^3/R_1^3 which seems the most useful.

Consider if this trend is consistent with a pressure-equalization mechanism. The equilibrium pressure inside the large bubble after its detachment is

$$P_1 = \frac{2\sigma}{R_1} + P_0, \tag{1}$$

where P_0 is the ambient water pressure including the hydrostatic pressure. The small bubble is still attached and growing at the instant of coalescence when sound emission occurs. Assuming it is growing spherically from a source of constant pressure, its internal pressure is

$$P_2(t) = \frac{2\sigma}{R_2} + P_0 + \rho_l\left[R_2\frac{\mathrm{d}^2R_2}{\mathrm{d}t^2} + \frac{3}{2}\left(\frac{\mathrm{d}R_2}{\mathrm{d}t}\right)^2\right], \tag{2}$$

in which the term in square brackets is due to the inertia of the liquid shell pushed outwards by the growing secondary bubble. It is easily derived from the principles of conservation of radial momentum and continuity applied to a cavity expanding in an infinite liquid domain. Hence, it also appears in bubble-acoustic equations (e.g. Rayleigh, 1917; Leighton, 1994), but here it merely refers to the inflation of the secondary bubble as air continues to flow into it, before the secondary bubble has contacted the primary bubble and volumetric oscillations have commenced. Viscous effects are small and are proportional to $\mathrm{d}R_2/\mathrm{d}t$ which will shortly be shown to be small itself. If the pressure-equalization explanation for the sound emission were valid, one would expect from (1) and (2) that the sound pressure amplitude would depend on P_1 and P_2 and hence on the seven parameters $R_1, R_2, \dot{R}_2, \ddot{R}_2, \sigma, P_0$ and ρ_l, where $\dot{R}_2$ denotes $\mathrm{d}R_2/\mathrm{d}t$ etc. There are three physical units, so dimensional analysis gives four dimensionless parameters, which are easily shown to be R_2/R_1, $P_0/(2\sigma/R_2)$ (or $P_0/(2\sigma/R_1)$), $\sqrt{(R_1\rho_l)/\sigma}\dot{R}_2$ and $(\sigma/(R_1^4\rho_l))\ddot{R}_2$. Since in the experiment P_0, ρ_l and σ were constant and R_1 was virtually constant, the results should depend on R_2/R_1 and possibly $\dot{R}_2$ and $\ddot{R}_2$.

The rate of growth of the secondary bubble, $\dot{R}_2$, can be calculated from the sequence of high-speed video frames, and Fig. 12 shows that the third term is weak compared to the first one. Because it is very small, the acceleration of the secondary bubble, $\ddot{R}_2$, is harder to estimate accurately; however, the measurements allow us to conclude that the last term of (2) is negligible.

Then (2) reduces to

$$P_2(t) \simeq \frac{2\sigma}{R_2} + P_0, \tag{3}$$

and the dimensional analysis assuming a pressure-equalization mechanism, predicts dependence on only two variables, (R_2/R_1) and $P_0/(2\sigma/R_2)$.

For an ideal gas, the internal energy contained in a bubble i of volume V_i at pressure P_i is $U_i = C_vP_iV_i$ (where C_v is the heat capacity at constant volume). Assuming that the coalescence process is adiabatic, the internal energy of the final bubble is the sum of the internal energies of the two initial bubbles, $U_3 = C_vP_3V_3 = C_v(P_1V_1 + P_2V_2)$. For $\alpha_V = V_2/V_1 \ll 1$, it yields

$$\Delta P = P_3 - P_1 = \alpha_V\frac{2\sigma}{R_2}. \tag{4}$$

From Fig. 11 it appears that most of the variation in the acoustic pressure amplitude was correlated with the dimensionless volume α_V of the small bubble, which is the cube of the dimensionless variable (R_2/R_1) at the instant of the small bubble's detachment. The data of Fig. 11 can be re-arranged, with the acoustic pressure P_{ac} scaled by the reference pressure $P_{ref} = 2\sigma/R_2$, and the resulting correlation is shown in Fig. 13.

The measured acoustic pressure is observed in Fig. 13 to be proportional to the pressure increase calculated by assuming that the internal energy of the small secondary bubble is suddenly released into the large primary, requiring a rapid pressure equalization,

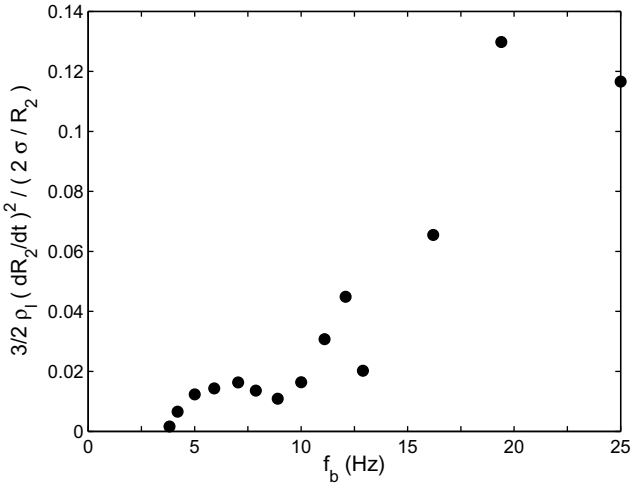

Fig. 12. Ratio of the components of secondary bubble internal pressure due to bubble-growth inertia at constant growth rate and due to Laplace pressure, as a function of the bubbling rate, f_b.

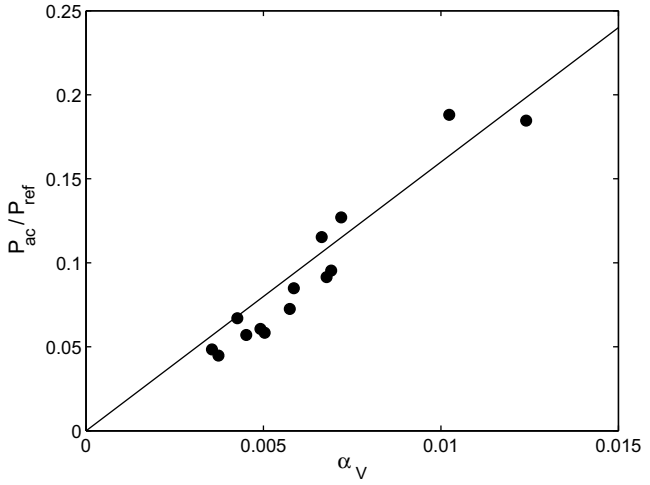

Fig. 13. Correlation between the scaled acoustic pressure amplitude P_{ac}/P_{ref} and dimensionless secondary bubble volume α_V. The line represents $P_{ac}/P_{ref} = 16\alpha_V$.

$$P_{ac} = k\Delta P, \tag{5}$$

where the constant k from the empirical fit to the data is close to 16. A value of k greater than unity implies that the measured energetics are greater than those theoretically predicted assuming $P_{ref} = 2\sigma/R_2$, a situation similar to that found by Pumphrey and Elmore (1990). However, it is clear that there is a good correlation with α_V. Careful and repeated audits of the signal acquisition and processing detailed in Section 2 confirmed that the measured amplitude and the assumptions leading to an estimate of its magnitude at the bubble surface could not result in an order of magnitude over-estimate. Since, as noted above, the primary bubble size does not change measurably during the experiments, the only parameters changed are the rate of production of bubbles and the size of the secondary bubble.

5. Conclusions

A system in which bubbles coalesced on formation generated loud bubble-acoustic emissions at the instant of coalescence of secondary bubbles with the primary bubble. Repeated coalescences issued repeated pulses of sound whereas events where bubbles merely 'kissed' did not. The amplitude of the emitted sound was up to an order of magnitude greater than the sound created on pinch-off of the primary bubble. The sound frequency was at the Minnaert frequency of the large bubble. As the air flow rate increased, the size and number of secondary bubbles increased, and the sound amplitude also increased. On coalescence, the sound pressure was found to always rise initially and its amplitude was shown to scale with the volume of the secondary bubble.

An analysis of the different timescales suggests that the best candidate for the sound-emission mechanism is the equalization of pressures in the coalescing bubbles. The higher Laplace pressure of the small bubble would pressurize the large bubble, and the fact that the pressure always rises is consistent with this. Previous authors (Longuet-Higgins, 1990; Pumphrey and Elmore, 1990) had also proposed a pressure-equalization mechanism, for bubble sounds due to drop impact, without satisfactory comparison with the experimentally measured amplitudes.

The measured sound amplitude was shown to be consistent with this mechanism since it is proportional to the pressure increase calculated by assuming that the internal energy of the small bubble is suddenly released in the large one. The constant of proportionality was an empirical fit to the data. The challenge now is to derive a theory that quantitatively predicts the magnitude of the actual experimental values. It can now be expected that the exact theory would feature the variable α_V, the dimensionless volume of the smaller secondary bubble.

It appears that the present experimental system generated data that scaled well owing to its high reproducibility, but did not allow control of the ratio of the volume of small bubble to that of the large one. In future work, a system should be designed that systematically coalesces pairs of different-sized bubbles that have both already separated from the gas supply system. Under these circumstances, both the volume and internal pressure of the bubbles could be controlled.

Acknowledgement

We are grateful to Sébastien Cazin at IMFT for technical help with the instrumentation and John Davy at CSIRO for valuable discussions.

References

Al-Masry, W.A., Ali, E.M., Aqeel, Y.M., 2005. Determination of bubble characteristics in bubble columns using statistical analysis of acoustic sound measurements. Chem. Eng. Res. Des. 83, 1196–1207.
Bhaga, D., Weber, M.E., 1980. In-line interaction of a pair of bubbles in a viscous liquid. Chem. Eng. Sci. 35, 2467–2474.
Boyd, J.W.R., Varley, J., 2001. The uses of passive measurement of acoustic emissions from chemical engineering processes. Chem. Eng. Sci. 56, 1749–1767.
Brüel & Kjaer, 2007. Product Data, Brüel & Kjaer Hydrophones – Types 8103, 8104, 8105 and 8106. Brüel & Kjaer, DK-2850 Nærum, Denmark.
Bui, A., Manasseh, R., 2006. A CFD study of the bubble deformation during detachment. In: Fifth International Conference on CFD in the Process Industries, Melbourne, Australia, 13–15 December 2006, Paper 053 1–6.
Chanson, H., Manasseh, R., 2003. Air entrainment processes of a circular plunging jet: void-fraction and acoustic measurements. J. Fluids Eng. 125, 910–921.
Chen, L., Manasseh, R., Nikolovksa, A., Norwood, C., 2003. Noise generation by an underwater gas jet. In: Proceedings, 8th Western Pacific Acoustics Conference, Melbourne, Australia, 7–9 April.
Clift, R., Grace, J.R., Weber, M.E., 1978. Bubbles, Drops and Particles. Academic Press, London.
Deane, G.B., Czerski, H., in press. A mechanism stimulating sound production from air bubbles released from a nozzle. J. Acoust. Soc. Am. Express Lett.
Ding, L., Farmer, D.M., 1994. Observations of breaking surface wave statistics. J. Phys. Oceanogr. 24, 1368–1387.
Doinikov, A.A., Zavtrak, S.T., 1995. On the mutual interaction of two gas bubbles in a sound field. Phys. Fluids 7, 1923–1930.
Doinikov, A.A., Manasseh, R., Ooi, A., 2005. On time delays in coupled multibubble systems. J. Acoust. Soc. Am. 117, 47–50.
Ellingsen, K., Risso, F., 2001. On the rise of an ellipsoidal bubble in water: oscillatory paths and liquid-induced velocity. J. Fluid Mech. 440, 235–268.
Farmer, D.M., Vagle, S., Booth, D., 2005. Reverberation effects in acoustical resonators. J. Acoust. Soc. Am. 118, 2954–2960.
Feuillade, C., 2001. Acoustically coupled gas bubbles in fluids: time-domain phenomena. J. Acoust. Soc. Am. 109, 2606–2615.
Goharzadeh, A., Mutabazi, I., 2001. Experimental characterization of intermittency regimes in the Couette–Taylor system. Eur. Phys. J. B 19, 157–162.
Hahn, T.R., Berger, T.K., Buckingham, M.J., 2003. Acoustic resonances in the bubble plume formed by a plunging water jet. Proc. R. Soc. Lond. A 459, 1751–1782.
Hsiao, P.-Y., Devaud, M., Bacri, J.-C., 2001. Acoustic coupling between two air bubbles in water. Eur. Phys. J. E 4, 5–10.
Hsi, R., Tay, M., Bukur, D., Tatterson, G.B., Morrison, G., 1985. Sound spectra of gas dispersion in an agitated tank. Chem. Eng. J. 31, 153–161.
Hu, Y.Y., Khoo, B.C., 2004. An interface interaction method for compressible multifluids. J. Comput. Phys. 198, 35–64.
Ida, M., 2002. A characteristic frequency of two mutually interacting gas bubbles in an acoustic field. Phys. Lett. A 297, 210–217.
Leighton, T.G., 1994. The Acoustic Bubble. Academic Press, London.
Leighton, T.G., Walton, A.J., 1987. An experimental study of the sound emitted by gas bubbles in a liquid. Eur. J. Phys. 8, 98–104.
Leighton, T.G., Fagan, K.J., Field, J.E., 1991. Acoustic and photographic studies of injected bubbles. Eur. J. Phys. 12, 77–85.
Leighton, T.G., Ramble, D.G., Phelps, A.D., Morfey, C.L., 1998. Acoustic detection of gas bubbles in a pipe. Acustica 84, 801–814.
Leighton, T.G., White, P.R., Morfey, C.L., Clarke, J.W.L., Heald, G.J., Dumbrell, H.A., Holland, K.R., 2002. The effect of reverberation on the damping of bubbles. J. Acoust. Soc. Am. 112, 1366–1376.
Loewen, M., Melville, W., 1991a. A model of the sound generated by breaking waves. J. Acoust. Soc. Am. 90, 2075–2080.

Loewen, M.R., Melville, W.K., 1991b. Microwave backscatter and acoustic radiation from breaking waves. J. Fluid Mech. 224, 601–623.
Longuet-Higgins, M.S., 1989a. Monopole emission of sound by asymmetric bubble oscillations. Part 1. Normal modes. J. Fluid Mech. 201, 525–541.
Longuet-Higgins, M.S., 1989b. Monopole emission of sound by asymmetric bubble oscillations. Part 2. An initial-value problem. J. Fluid Mech. 201, 543–565.
Longuet-Higgins, M.S., 1990. An analytic model of sound production by raindrops. J. Fluid Mech. 214, 395–410.
Longuet-Higgins, M.S., Kerman, B.R., Lunde, K., 1991. The release of air bubbles from an underwater nozzle. J. Fluid Mech. 230, 365–390.
Manasseh, R., 1996. Bubble-pairing phenomena in sparging from vertical-axis nozzles. In: 24th Australian & NZ Chemical Engineering Conference, Sydney, 30 September–2 October, vol. 5, pp. 27–32.
Manasseh, R., Yoshida, S., Rudman, M., 1998. Bubble formation processes and bubble acoustic signals. In: Third International Conference on Multiphase Flow, Lyon, France, 8–12 June.
Manasseh, R., LaFontaine, R.F., Davy, J., Shepherd, I.C., Zhu, Y., 2001. Passive acoustic bubble sizing in sparged systems. Exp. Fluids 30, 672–682.
Manasseh, R., Nikolovska, A., Ooi, A., Yoshida, S., 2004. Anisotropy in the sound field generated by a bubble chain. J. Sound Vib. 278, 807–823.
Manasseh, R., Babanin, A., Forbes, C., Rickards, K., Bobevski, I., Ooi, A., 2006. Passive acoustic determination of wave-breaking events and their severity across the spectrum. J. Atmos. Ocean Tech. 23, 599–618.
Melville, W.K., Loewen, M., Felizardo, F., Jessup, A., Buckingham, M., 1988. Acoustic and microwave signatures of breaking waves. Nature 336, 54–56.
Minnaert, M., 1933. On musical air bubbles and the sound of running water. Phil. Mag. 16, 235–248.
Nevers, N.D., Wu, J.-L., 1971. Bubble coalescence in viscous fluids. Am. Inst. Chem. Eng. J. 17, 182–186.
Nikolovska, A., 2005. Passive acoustic transmission and sound channelling along bubbly chains. Department of Mechanical and Manufacturing Engineering, University of Melbourne, Australia.
Nikolovska, A., Manasseh, R., Ooi, A., 2007. On the propagation of acoustic energy in the vicinity of a bubble chain. J. Sound Vib. 306, 507–523.
Oğuz, H., Prosperetti, A., 1993. Numerical calculation of the underwater noise of rain. J. Fluid Mech. 228, 417–442.
Prosperetti, A., 1988. Bubble-related ambient noise in the ocean. J. Acoust. Soc. Am. 84, 1042–1054.
Prosperetti, A., Oğuz, H., 1993. The impact of drops on liquid surfaces and the underwater noise of rain. Ann. Rev. Fluid Mech. 25, 577–602.
Pumphrey, H.C., Crum, L.A., 1990. Free oscillations of near-surface bubbles as a source of the underwater noise of rain. J. Acoust. Soc. Am. 87, 142–148.
Pumphrey, H.C., Elmore, P.A., 1990. The entrainment of bubbles by drop impacts. J. Fluid Mech. 220, 539–567.
Rayleigh, 1917. On the pressure developed in a liquid during the collapse of a spherical cavity. Phil. Mag. 34, 94–98.
Stewart, C.W., 1995. Bubble interaction in low-viscosity liquids. Int. J. Multiphase Flow 21, 1037–1046.
Strasberg, M., 1953. The pulsation frequency of nonspherical gas bubbles in liquid. J. Acoust. Soc. Am. 25, 536–537.
Strasberg, M., 1956. Gas bubbles as sources of sound in liquid. J. Acoust. Soc. Am. 28, 20–26.
Tolstoy, I., 1986. Superresonant systems of scatterers. I. J. Acoust. Soc. Am. 80, 282–294.
Yoshida, S., Manasseh, R., Kajio, N., 1998. The structure of bubble trajectories under continuous sparging conditions. In: 3rd International Conference on Multiphase Flow, Lyon, France, June 1998, pp. 426 1–8.
Zabolotskaya, E.A., 1984. Interaction of gas bubbles in a sound field. Sov. Phys. Acoust. 30, 365–368.